Particles II

Access the latest eBook →

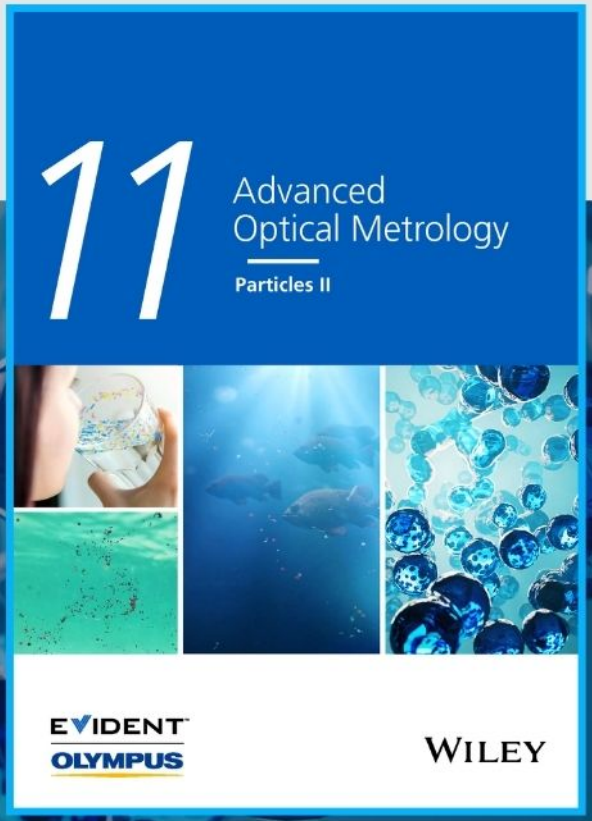

Impact on Biological Systems and the Environment

This eBook is dedicated to the research of Professor David Wertheim.
In collaboration with various groups, Professor Wertheim uses confocal microscopy to analyse the impact of different types of particles on human health and the environment, with a focus on human health-hazardous particles detected with solid-state nuclear track detectors (SSNTD). Download for free, today.

EVIDENT
OLYMPUS

WILEY

ADVANCED FUNCTIONAL MATERIALS
www.afm-journal.de

Enhanced Condensation on Soft Materials through Bulk Lubricant Infusion

*Chander Shekhar Sharma, Athanasios Milionis, Abhinav Naga, Cheuk Wing Edmond Lam, Gabriel Rodriguez, Marco Francesco Del Ponte, Valentina Negri, Hopf Raoul, Maria D'Acunzi, Hans-Jürgen Butt, Doris Vollmer, and Dimos Poulikakos**

Soft substrates enhance droplet nucleation during water vapor condensation because their deformability inherently reduces the energetic threshold for heterogeneous nucleation relative to rigid substrates. However, this enhancement is counteracted later in the condensation cycle, when substrate viscoelastic dissipation inhibits condensate droplet shedding. Here a polydimethylsiloxane (PDMS) based organogel is designed to overcome this limitation. It is shown that merely 5% bulk lubricant infusion in PDMS reduces viscoelastic dissipation in the substrate by nearly 28 times while doubling the droplet nucleation density. Parameters for water condensation on this organogel are correlated with material properties controlled by design, i.e., fraction and composition of uncrosslinked chains and shear modulus. It is demonstrated that the increase in nucleation density and reduction in precoalescence droplet growth rate is rather insensitive to the lubricant percentage in PDMS within the broad range investigated. These results indicate the presence of a lubricant layer on the substrate surface that cloaks the growing condensate droplets. This cloaking effect is visualized, and it is shown that cloaking occurs significantly faster on PDMS if it is infused with bulk lubricant. Overall, bulk lubricant infusion in PDMS enhances condensation and leads to a more than 40% higher dewing on the substrate.

1. Introduction

Condensation of water vapor on a colder surface is a widely observed phenomenon and manifests itself visibly to the human eye, for example, as fogged windscreens or glasses on a humid day. In industry, condensation is critical in multiple applications such as power generation,[1] water desalination,[2] and dew water harvesting[3,4] and thermal management.[5] Tuning and predicting the outcome of condensation is challenging because of the interplay of several processes. It is well established that condensation of a fluid on rigid substrates proceeds in four distinct steps – formation of initial condensate nuclei, growth of individual droplets through direct condensation, droplet coalescence, and eventual removal of the condensate from the surface.[6] On hydrophilic substrates, coalescence of the individual droplets usually results in a continuous condensate film. However, efficient condensation requires that the fluid condenses as distinct droplets that rapidly shed from the surface.[7] This condensation mode can be realized by hydrophobizing the substrate through the modification of the surface roughness and chemistry. Depending on the degree of hydrophobicity and morphology of the surface texture, condensate droplets can be shed by multiple mechanisms such as gravity-induced depinning,[7] coalescence induced droplet jumping,[8–13] cascading coalescence,[3,4] and Laplace pressure gradients.[14–18] However, this enhanced condensate droplet shedding on rigid hydrophobic substrates is

C. S. Sharma
Thermofluidics Research Lab
Department of Mechanical Engineering
Indian Institute of Technology Ropar
Rupnagar, Punjab 140 001, India

The ORCID identification number(s) for the author(s) of this article can be found under https://doi.org/10.1002/adfm.202109633.

© 2021 The Authors. Advanced Functional Materials published by Wiley-VCH GmbH. This is an open access article under the terms of the Creative Commons Attribution-NonCommercial-NoDerivs License, which permits use and distribution in any medium, provided the original work is properly cited, the use is non-commercial and no modifications or adaptations are made.

DOI: 10.1002/adfm.202109633

A. Milionis, C. W. E. Lam, G. Rodriguez, M. F. Del Ponte, V. Negri, D. Poulikakos
Laboratory of Thermodynamics in Emerging Technologies
Department of Mechanical and Process Engineering
ETH Zurich
Zurich 8092, Switzerland
E-mail: dpoulikakos@ethz.ch

A. Naga, M. D'Acunzi, H.-J. Butt, D. Vollmer
Max Planck Institute for Polymer Research
Ackermannweg 10, D-55128 Mainz, Germany

H. Raoul
Institute of Mechanical Systems, Department of Mechanical and Process Engineering
ETH Zurich
Zurich 8092, Switzerland

 © 2021 The Authors. Advanced Functional Materials published by Wiley-VCH GmbH

achieved at the cost of reduced nucleation density compared to hydrophilic substrates, which is a critical limitation for water harvesting applications.[19,20]

Soft solid substrates such as Polydimethylsiloxane (PDMS) overcome the limitation concerning nucleation density by lowering the energetic threshold for heterogeneous nucleation. This is because the condensate droplets can trigger substrate deformation through elastocapillary effects and reduce the overall energy of the system consisting of substrate-water and water-water vapor interfaces.[21,22] Unfortunately, this increase in nucleation density is achieved at the cost of reduced droplet mobility due to the formation of a distinct wetting ridge around the droplet.[23] As the droplet slides, this wetting ridge causes viscoelastic dissipation within the substrate, otherwise known as viscoelastic braking.[24] This effect can be far more significant than the viscous dissipation within the liquid condensate droplets, thereby making the material properties of the soft substrate the governing factor behind the inhibited motion of the droplets.[23,25]

The above-described characteristics of high condensate nucleation density but inhibited droplet movement on soft substrates highlight a quandary for practical applications of soft substrates in condensation applications, specifically water harvesting from humid air. In recent years, slippery, lubricant-infused rigid textures have been reported, potentially addressing the dilemma mentioned above.[26,27] Such a hybrid texture can present enhanced nucleation density and rapid shedding of condensate droplets due to low contact angle hysteresis.[28–30] However, lubricant-infused textures may be limited by the gradual draining of the thin lubricant layer from the micro and nanometric surface features.[29,31]

Here, we design a PDMS-based organogel to achieve high nucleation density while maintaining a high rate of droplet shedding. Our approach involves increasing the fraction of uncrosslinked chains within the substrate through the bulk infusion of a lubricant. The resulting organogel[32] allows controlled reduction in viscoelastic dissipation in PDMS samples while retaining the inherently high droplet nucleation density. We perform careful material characterization of the substrates and *in-situ* micro- and macroscale investigations of condensation. We find that this adjustment of the proportion of uncrosslinked chains directly influences all the three key processes in the heterogeneous dropwise condensation cycle – namely droplet nucleation, droplet growth, and droplet shedding from the surface. The uncrosslinked chains slowly diffuse outwards, forming a layer of lubrication. This lubricant layer enhances droplet movement on the surface[33–36] and increases droplet nucleation during condensation. However, it also results in the cloaking of condensed drops, thereby lowering the individual microdroplet growth rate. Overall, however, the enhancement in droplet nucleation and sliding more than compensate for any reduction in droplet growth rate, resulting in a significant enhancement in water condensation rate. We provide experimental evidence for this enhancement in terms of condensate water collection. PDMS substrates with bulk lubricant infusion condense more than 40% more water than conventional PDMS substrate under similar dewing conditions. We also systematically characterize the various material properties that affect the overall condensation process — material stiffness characterization through bulk stiffness and wetting ridge height measurements, the fraction of uncrosslinked chains and molecular weight distribution through Gel Permeation Chromatography (GPC), and material viscoelasticity through precise measurements of droplet sliding speeds on the substrate. Our work puts forth PDMS based organogels as a potential facile pathway towards enhanced condensation on soft substrates for water harvesting through dewing.

2. Results and Discussion

2.1. Substrate Elastocapillarity and Composition

We prepared a series of soft substrates with a range of stiffness and fraction of uncrosslinked chains by varying the PDMS (Sylgard 184, Dow Corning) base to curing agent (crosslinker) ratio and adding lubricant (silicone oil, Xiameter PMX 200, 100 cSt, Credimex Inc.) prior to curing. In the following, each substrate is designated as 'PxLy' where 'x' is the base to crosslinker ratio, i.e., $x = Ba/Cr$ and 'y' is the percentage by weight of lubricant defined as $y = 100Lu/(Lu + Cr(1 + x))$. Here, Ba, Lu and Cr are the weights of base, lubricant and crosslinker in the uncured mixture, respectively. For example, while P10L0 represents PDMS with a 10:1 base to crosslinker ratio and no additional silicone oil lubricant, P10L5 represents PDMS with the same base to crosslinker ratio but 5% lubricant added by weight. Table S1 in the Supporting Information lists the composition of all substrates considered in this work.

Water droplets condensed on soft substrates pull the substrate at the contact line while the substrate is depressed in the contact area between the droplet and the substrate due to Laplace pressure. The three interfacial tensions, γ_{sl}, γ_{sv}, and γ_{lv} balance in a Neumann's triangle configuration at the contact line and a wetting ridge is formed around the droplet.[37,38] This wetting ridge influences the droplet coalescence and shedding process during condensation on soft substrates.[21] Here, γ_{sl}, γ_{sv}, and γ_{lv} represent surface tensions for solid-liquid, solid-vapor and liquid-vapor interfaces. Since the wetting ridge formation is dependent on substrate elasticity, we characterized the elasticity of each sample by using a micro-indentation test. We also independently characterized the wetting ridge formation by measuring the wetting ridge height using white light interferometry.[39]

Figure 1a shows the range of substrate elasticities and the corresponding wetting ridge heights explored. The wetting ridge height increases for softer substrates as it scales as $\approx\gamma\sin(\theta)/G$, where γ is the liquid-vapor interfacial tension, G is the shear modulus, and θ is the apparent contact angle with respect to the undeformed surface of the substrate. The wetting ridge height increases from ≈100 nm to ≈1.4 µm as the shear modulus is reduced from ≈500 to ≈15 kPa (Figure 1a). This is in line with the previously reported trends about large wetting ridge heights formed on soft surfaces.[21] It is evident that the substrate with stoichiometric base to crosslinking ratio (10:1) is stiffer than the ones with non-stoichiometric ratios (see P10L0 vs. P1L0 and P40L0). Additionally, irrespective of the base to crosslinker ratio, the addition of lubricant to the bulk results in reduced stiffness of the cured polymer (for example, compare

© 2021 The Authors. Advanced Functional Materials published by Wiley-VCH GmbH

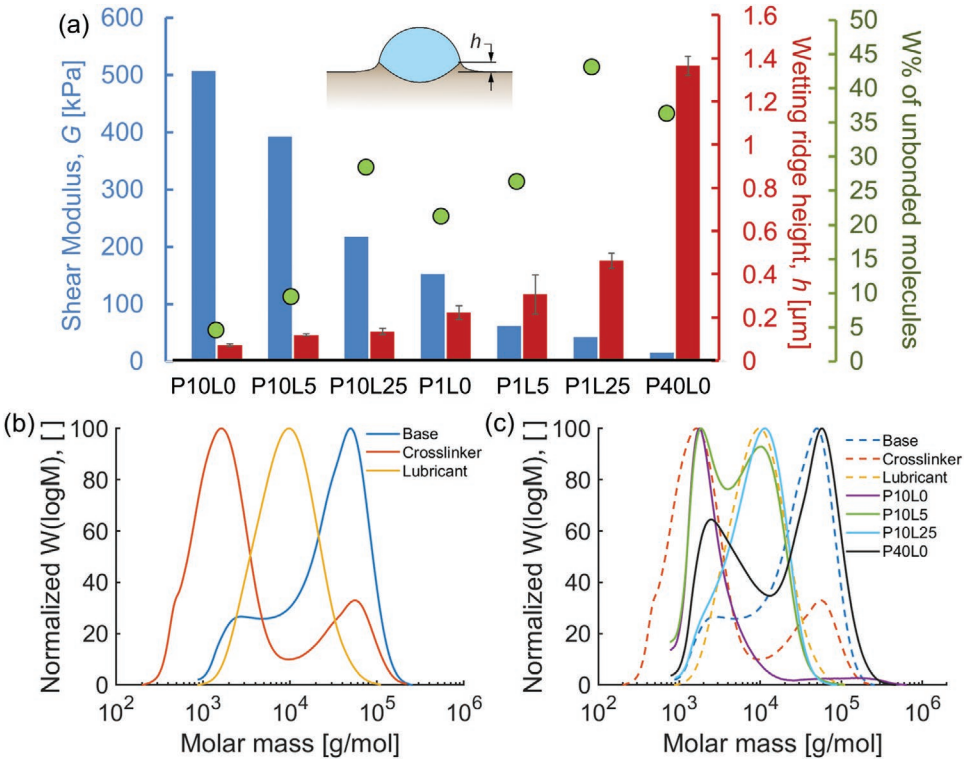

Figure 1. a) Shear modulus (blue bars), wetting ridge heights (red bars), and percentage by weight of uncrosslinked chains (green dots) for the soft substrates. Inset figure defines the wetting ridge height (*h*), as measured by white light interferometry. For all substrates, wetting ridge height is measured using droplets of volume ≈ 12 µL or larger. Each substrate is designated as 'PxLy' where 'x' is the base to crosslinker ratio and 'y' is the percentage by weight of lubricant in the substrate. Substrates with lower shear modulus result in larger wetting ridge height. Deviation from stoichiometric base-to-crosslinker ratio and addition of lubricant results in a larger fraction of uncrosslinked chains. b) GPC of precursors showing molecular weight distribution of uncrosslinked chains in base, crosslinker, and lubricant. c) Molecular weight distribution of uncrosslinked chains in P10L0, P10L5, P10L25 and P40L0 (solid curves) overlaid on the distributions for precursors shown in (b) (dashed curves). Corresponding distribution for P1L0, P1L5, and P1L25 are shown in Figure S1 in the Supporting Information.

P10L0 to P10L5 and P10L25). Thus, deviation from stoichiometric mixing ratios as well as bulk lubricant infusion reduces the shear modulus of the substrate.

Even after curing, PDMS samples contain uncrosslinked chains.[36,40,41] We determined the relative amount and the molecular weight distribution of the uncrosslinked chains by dissolving out the oligomers. Figure 1a shows the percentage of uncrosslinked chains as extracted by swelling in toluene. We observe that for a given ratio of base to crosslinker, the percentage of uncrosslinked chains increases with bulk lubricant infusion (for instance, compare P10L0 with P10L5, and P10L25 and P1L0 with P1L5 and P1L25). Additionally, for any percentage of the lubricant, deviation from stoichiometric base to crosslinker ratio results in a higher percentage of uncrosslinked chains (for instance, compare P10L0 with P1L0 and P40L0, and P10L5 with P1L5).

Next, we characterize the composition of uncrosslinked chains in various samples through GPC analysis as, apart from the fraction of uncrosslinked chains, the composition of such chains is also likely to affect the viscoelastic dissipation from the substrate. Figure 1b shows results of GPC analysis of the three precursors used in the fabrication of samples – two components of the Sylgard 184 kit, i.e., base and crosslinker, and lubricant (Credimex Xiameter Silicone oil). The molecular weight distribution of the three components is significantly different. The lubricant Credimex has a unimodal molecular weight distribution centered around 10^4 g mol^{-1}. Both the base and the crosslinker have a bimodal molecular weight distribution. The main peak of the crosslinker is centered around 1.6×10^3 g mol^{-1}. However, the crosslinker also contains a small fraction of high molecular weight components, which are centered around 6×10^4 g mol^{-1}. The molecular weight distribution of the base is centered around 5×10^4 g mol^{-1}. However, the base also contains a small fraction of molecules having a molecular weight as low as 10^3 g mol^{-1}.

Figure 1c shows the molecular weight distributions of uncrosslinked chains for the substrates P10L0, P10L5 and P10L25 overlaid on the distributions shown in Figure 1b. P10L0 does not contain Credimex. Since the peak is centered around 1.7×10^3 g mol^{-1}, the uncrosslinked chains in P10L0 are due to the low molecular weight components of the base and of crosslinker. Both, the uncrosslinked chains in P10L5 and P10L25 show a peak centered around 6×10^4 g mol^{-1}, which can be assigned to the added lubricant. In case of P10L5, the second peak centered around 1.7×10^3 g mol^{-1} corresponds to the peak observed for the position of the low molecular weight peak of the crosslinker. However, the low molecular weight components of the Sylgard Base may also contribute to this peak.

© 2021 The Authors. Advanced Functional Materials published by Wiley-VCH GmbH

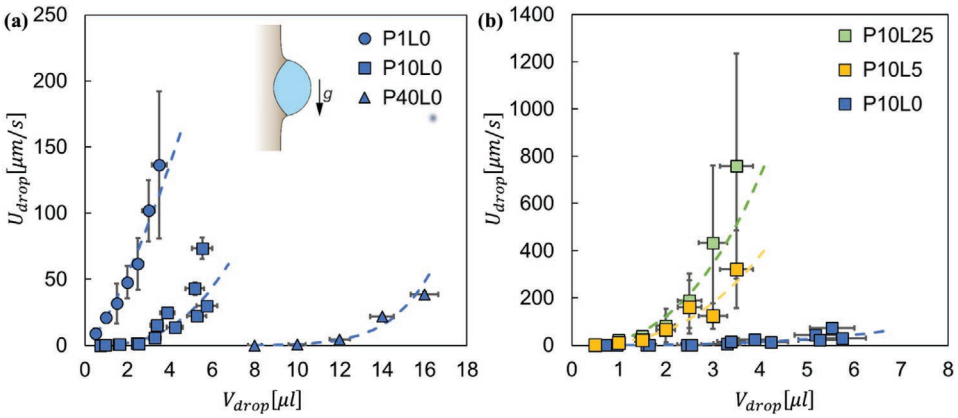

Figure 2. a) Comparison of droplet sliding velocities as a function of droplet volume for P10L0, P1L0, and P40L0. Inset figure shows a schematic of drop sliding on the substrate under gravity. b) Similar comparison for P10L0, P10L5, and P10L25. Higher sliding velocities for a given droplet volume indicate lower viscoelastic braking in the substrate. Dotted lines represent curve fits with $U_{drop} = \frac{U_0}{V_0^{2/3m}} V_{drop}^{2/3m}$ where V_0, U_0 and m are fitting parameters. Values of these parameters are listed in Table S2 in the Supporting Information .

The uncrosslinked molecules in P10L25 mainly result from the lubricant. (Refer Supporting Information Section S1 for results of GPC analysis for P1L0, P1L5, and P1L25). In essence, the above analysis indicates that the mobile uncrosslinked chains in these PDMS substrates are dominated by the low molecular weight components of crosslinker and base and by the additional lubricant. The only exception here is P40L0 wherein, as illustrated in Figure 1c, the high molecular weight components dominate the molecular weight distribution of uncrosslinked chains. The P40L0 peak centered around 5.8×10^5 g mol^{-1} is contributed mainly by the large proportion of base in the substrate with smaller contribution from crosslinker.

2.2. Substrate Viscoelasticity

Droplets sliding down a vertical soft substrate attain a terminal velocity when the viscoelastic dissipation balances the work done by the driving force of droplet weight.[24] Measuring this velocity for droplets of various volumes provides an estimation of the inherent viscoelastic dissipation in the substrate. **Figure 2**a compares droplet velocity (U_{drop}) as a function of droplet volume (V_{drop}) for P10L0, P1L0, and P40L0, i.e., PDMS of varying base to crosslinker ratio and no additional lubricant infusion. Sliding droplets of same size attain higher sliding velocities on P1L0 than P10L0 and lower sliding velocities on P40L0 than P10L0. Figure 2b shows the same comparison for P10L0, P10L5 and P10L25, i.e., PDMS substrates with same base to crosslinker ratio but varying additional lubricant percentage. Here, sliding droplets on substrates with bulk lubricant infusion, P10L5 and P10L25, attain much higher velocities than P10L0. Moreover, this increase in sliding velocity over P10L0 is much higher than that obtained in the case of P1L0 in Figure 2a. This clearly indicates that bulk lubricant infusion results in a significant reduction in viscoelastic dissipation in soft substrates. A comparison of Figure 2 and Figure 1 leads to three conclusions. First, viscoelastic dissipation can be reduced by infusing the PDMS with lubricant despite the fact than lubricant infused substrates have lower shear modulus (and thus larger wetting ridge formation) than P10L0. As shown by GPC analysis in Figure 1c, lubricant infused in P10L5 and P10L25 contributes to uncrosslinked chains and makes the substrate more slippery. Second, while viscoelastic dissipation can be reduced by increasing the proportion of crosslinker (see P1L0 vs P10L0 in Figure 2a), this reduction is much less significant than obtained by infusing lubricant in PDMS P10L0. And third, as alluded to in section 2.1, viscoelastic dissipation depends not only on the fraction of uncrosslinked chains but also on the composition of the chains. This is most notably illustrated by P40L0 which has a much higher fraction of uncrosslinked chains than P10L0, P10L5 and P10L25 (Figure 1a), yet viscoelastic dissipation is higher in P40L0. It is likely that the dominance of high molecular weight components in the uncrosslinked chains in P40L0, in combination with large wetting ridge height, results in high viscoelastic dissipation during droplet sliding on P40L0.

In Figures 2a,b, dashed lines are curve fits based on an energy model. This model assumes that the work done by the weight of sliding drop is mainly dissipated through viscoelastic braking by the substrate. Although droplets sliding on PDMS infused with lubricant may also experience viscous dissipation from a layer of lubricant formed on the top surface of the sample,[42] it is difficult to distinguish between the viscous dissipation from lubricant and viscoelastic dissipation from the elastomer. In essence, the viscoelastic dissipation in our model represents the net energy dissipation caused by the substrate. The drop sliding velocity, U_{drop} can be related to volume of drop, V_{drop} as.[24]

$$U_{drop} = \frac{U_0}{V_0^{2/3m}} V_{drop}^{2/3m} \quad where\ V_0 = \left(\frac{2\gamma^2 I}{\pi \rho g G h f^{\frac{1}{3}}(\theta)} \right)^{3/2} \tag{1}$$

Here, ρ and γ are density and surface tension of the liquid respectively, θ is the apparent contact angle and U_0 and m are rheological constants for a substrate. For each substrate, U_0 and m are obtained by fitting the experimental data for U_{drop} as a function of V_{drop}. The dashed lines in Figure 2 are plots of the

© 2021 The Authors. Advanced Functional Materials published by Wiley-VCH GmbH

above equation. Next, in order to quantitatively estimate differences in viscoelastic dissipation among different substrates, we compare the ratio of viscoelastic dissipation in the substrate due to the movement of the contact line $(\dot{D}_{ve})$ to viscous dissipation $(\dot{D}_{v})$ within the droplet. This dissipation ratio is given by[24,39]

$$\frac{\dot{D}_{ve}}{\dot{D}_{v}} = \frac{\gamma^2 U_{drop}^{m-1} I \theta}{3\pi^2 G h \mu U_0^m l} \tag{2}$$

This ratio is lower for more slippery soft substrates. Here, μ is the viscosity of the liquid and I and l are constants based on droplet morphology.

Based on the droplet sliding measurements and the resulting curve fits shown in Figure 2b, we estimate that, relative to P10L0, $\frac{\dot{D}_{ve}}{\dot{D}_{v}}$ reduces by a factor of ≈28 for P10L5 and ≈57 for P10L25 for a 5µL drop, thus indicating a large reduction in viscoelastic dissipation for lubricant infused substrates. However, on P1L0 the addition of lubricant did not result in any significant change in viscoelastic dissipation, unlike the case of P10L0, indicating that bulk lubricant infusion in stoichiometric base-to-crosslinker composition provides the most benefit in terms of achieving slippery soft surfaces. In other words, lubricant addition facilitates sliding on sufficiently cross-linked PDMS (i.e., PDMS with stoichiometric base to crosslinker ratio). This is likely due to the much larger relative contribution of crosslinker to uncrosslinked chains in P1L5 and P1L25 compared to P10L5 and P10L25 (Figure 1c; Figure S1, Supporting Information). Refer to Section S2 in the Supporting Information for details of the model fit, estimation of the dissipation ratio and comparison of droplet sliding velocities for P1L0, P1L5, and P1L25.

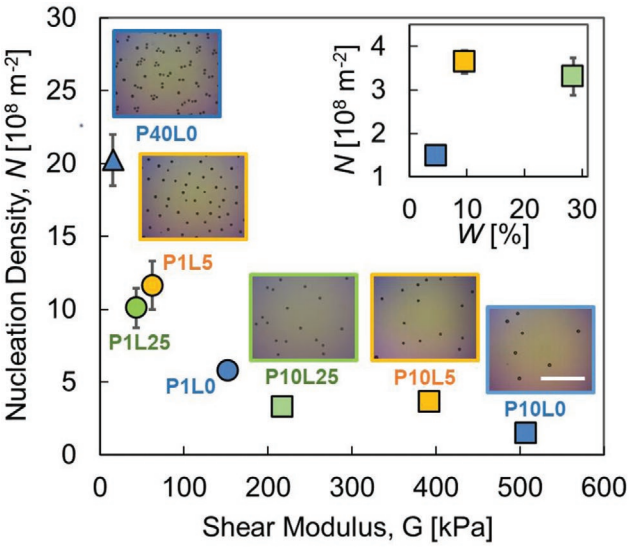

Figure 3. Nucleation density of condensation on various substrates at 100% humidity and room temperature as a function of substrate shear modulus. Squares correspond to substrates with 10:1 base to crosslinker ratio (i.e., P10L0, P10L5, and P10L25), circles correspond to substrates with 1:1 base to crossslinker ratio (i.e., P1L0, P1L5, and P1L25). Inset figures show typical condensation nucleation densities on five substrates over an observation area of 235 µm x 191 µm. The scale bar (in white) represents 100 µm. Inset plot shows nucleation density as a function of percentage of uncrosslinked chains for P10L0, P10L5, and P10L25.

2.3. Microscale Condensation

Microscale *in-situ* condensation observations were performed that yielded quantitative information on nucleation and subsequent growth of condensate droplets on various substrates. **Figure 3** shows nucleation density (N) of heterogeneous condensation as a function of the substrate shear modulus. Overall, the nucleation density follows an inverse relation with substrate shear modulus[21,43] wherein N changes more steeply at lower shear modulus values. Additionally, substrates with bulk lubricant infusion achieve higher nucleation density. This is evident from comparison of N for P10L0 with P10L5 and P10L25, and similarly from comparison of P1L0 against P1L5 and P1L25. Interestingly however, we find that for substrates with bulk lubricant infusion, N values show minimal dependence on the percentage of lubricant infused in the material. For instance, P10L5 and P10L25 achieve nearly similar nucleation density despite the fact that the shear modulus for P10L25 is nearly 50 percent lower and fraction of uncrosslinked chains is nearly 200 percent higher (inset plot in Figure 3) than that for P10L5. Based on this insensitivity of N value to change in bulk lubricant concentration, we speculate that the lubricant-dominated uncrosslinked chains in these substrates (see Figure 1c and Figure S1 (Supporting Information)) diffuse outwards from the bulk and induce the formation of a continuous layer of lubricant on the top surface of the substrate. This lubricant layer in turn governs the nucleation dynamics during condensation, irrespective of the amount of lubricant present in the bulk of the material.

Figure 4a shows precoalescence growth of condensate droplets for P10L0, P10L5 and P10L25 as a function of observation time. Each curve is an average of growth curves of three different randomly chosen droplets for the respective substrates. The observation is initiated when first droplets become visible at the limit of resolution of the optical system. The observation is continued while the temperature of the cooling stage is held constant at 20 °C and the humidity and temperature in the experimental chamber are maintained at 100% and 28.7 °C respectively. Interestingly, the droplet growth rate for non-lubricated P10L0 is higher than that for the lubricated samples P10L5 and P10L25. Thus, while the lubricated substrates show higher performance than P10L0 in terms of nucleation density, the opposite is true in terms of droplet growth. Figure 4b presents snapshots of the condensate droplet growth process on P10L0 and P10L5 demonstrating the slower droplet growth for P10L5. Moreover, the droplets grow at nearly the same rate on P10L5 and P10L25 even though P10L25 has nearly 5 five times more lubricant, and thus shows increased substrate deformability, than P10L5. This similarity of droplet growth, along with the earlier stated similarity in nucleation density for these widely different lubricant concentrations, again indicates that the condensation dynamics for lubricated substrates are governed by a surface characteristic that dominates the large difference in bulk material properties. As already alluded to, we believe

© 2021 The Authors. Advanced Functional Materials published by Wiley-VCH GmbH

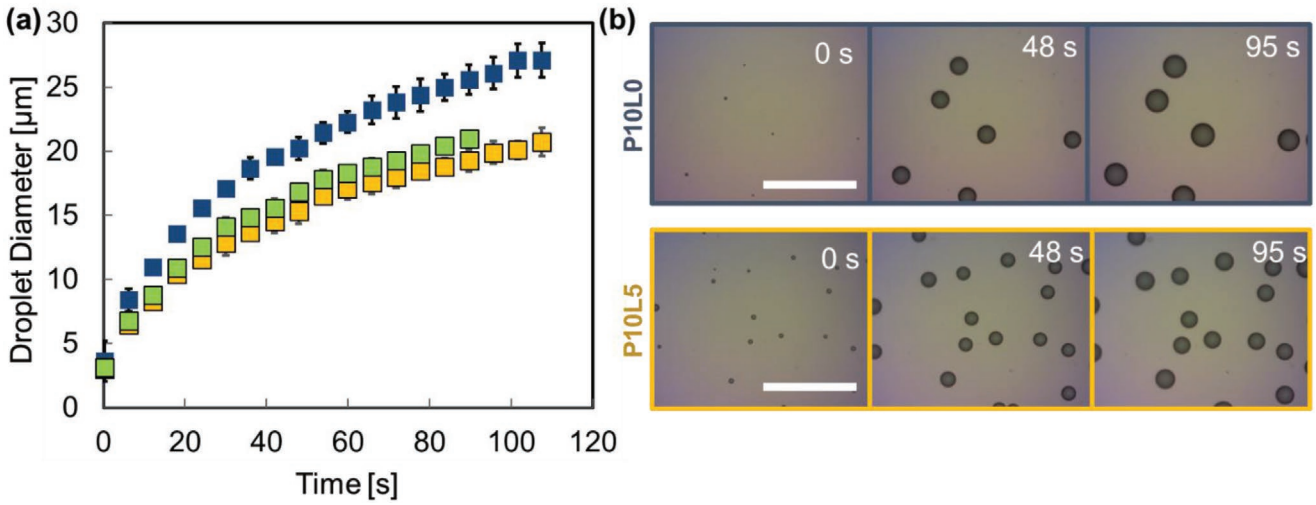

Figure 4. a) Comparison of precoalescence condensate droplet growth rate on substrates without (P10L0) and with (P10L5 and P10L25) bulk lubricant infusion. b) Snapshots of condensation on P10L0 and P10L5 at equivalent time-instants after the start of nucleation, under same atmospheric humidity and surface subcooling conditions. Scale bars in white represent 100 μm.

that this surface property is the existence of a distinct layer of lubricant formed on the surface by the outwards diffusion of the lubricant from the bulk elastomer matrix. The presence of this lubricant layer controls the nucleation density as well as the condensate droplet growth rate. The comparison of precoalescence droplet growth rate between P1L0, P1L5 and P1L25 is similar to the comparison between P10L0, P10L5, P10L25 (Refer Figure S3a in the Supporting Information). P1L5 and P1L25 show similar and lower droplet growth rate compared to P1L0. A comparison of all substrates shows that overall, P1L5, P1L25 show lower droplet growth rates than P10L5 and P10L25, and P40L0 shows the minimum droplet growth rate (Figure S3b, Supporting Information).

The reduced condensate droplet growth rate for substrates with bulk lubricant infusion can arise from a combination of two factors: a) higher nucleation density[44,45] and b) formation of a cloaking layer over the droplets, similar to the case of lubricant-infused rigid textures.[29,46] The higher nucleation density can impose diffusion limitation on condensate droplet growth rate due to close spacing between droplets and resulting distortion of the vapor concentration field.[47] If the droplets get cloaked by lubricant, it has been speculated that this cloak may form a barrier for diffusion of water molecules from vapor to liquid, thus slowing the overall process of phase change.[28,29] (Refer Section S3 in the Supporting Information for further details).

2.4. Detection of Cloaking Layer and Cloaking Kinetics

For the lubricant used, i.e., Xiameter PMX 200/100cs Silicone oil, cloaking of water droplets is energetically favourable as, it has a positive spreading coefficient on water ($S = \gamma_{wv} - \gamma_{lv} - \gamma_{lw} > 0$), where γ_{lv}, γ_{lw}, and γ_{wv} are the interfacial tensions for lubricant-air, lubricant-water and water-air interfaces.[48] Thus an oil cloaking layer with thickness below 100 nm would be formed on the condensing drops.[29,46]

To confirm the formation of a cloaking layer on water droplets, we imaged 0.3 μL sized drops placed on P10L0 and P10L25 using confocal microscopy (**Figure 5**, taken around 30 min after placing the drop). A side view cross section of the cloak (PDMS, orange) is shown in Figure 5d, with the relevant region highlighted in the schematic drawn in Figure 5e. Figure 5a–c shows the top part of the drop. Fluorescent signal from the glycerol/water drop is shown in blue [Figure 5a] and fluorescence from the untethered chains diffusing from the substrate and cloaking the drop is shown in orange [Figure 5b]. These two signals are overlaid into a single image in Figure 5c. While the drops were initially bare without any observable lubricant cloak, after around 30 min, they became cloaked by material from the substrates for both P10L0 and P10L25. This shows that irrespective of the concentration of the additional lubricant, the drops are ultimately cloaked. While for P10L0 this cloaking proceeds by the diffusion of the uncrosslinked Sylgard 184 chains from the substrate, for P10L25, it is a combination of both the diffusion of the uncrosslinked Sylgard 184 chains and the diffusion of the added lubricant (Xiameter).

While confocal microscopy confirms the formation of cloaking layer on water droplets, it does not provide reliable quantitative information on how fast the cloaking proceeds on various substrates. Cloaking is expected to reduce the surface tension of the drop. Therefore, to quantify differences in the cloaking kinetics due to lubricant infusion in PDMS, we measured the change in drop-air interfacial tension of a water drop placed into contact with P10L0, P10L5, and P10L25 as follows.[49] A glass slide with a 2 mm diameter hole was spin-coated with the PDMS mixture [**Figure 6**a]. A 38 μL drop of pure water was positioned in pendant configuration such that its three-phase contact line was pinned at the edge of the hole. This is to ensure that the contact line does not slide on the substrate as the interfacial tension of the drop changes (refer Section S4 in the Supporting Information for further experimental details). Initially, the drop's interface consists of water molecules surrounded by vapor (air), resulting in a surface tension equal to

© 2021 The Authors. Advanced Functional Materials published by Wiley-VCH GmbH

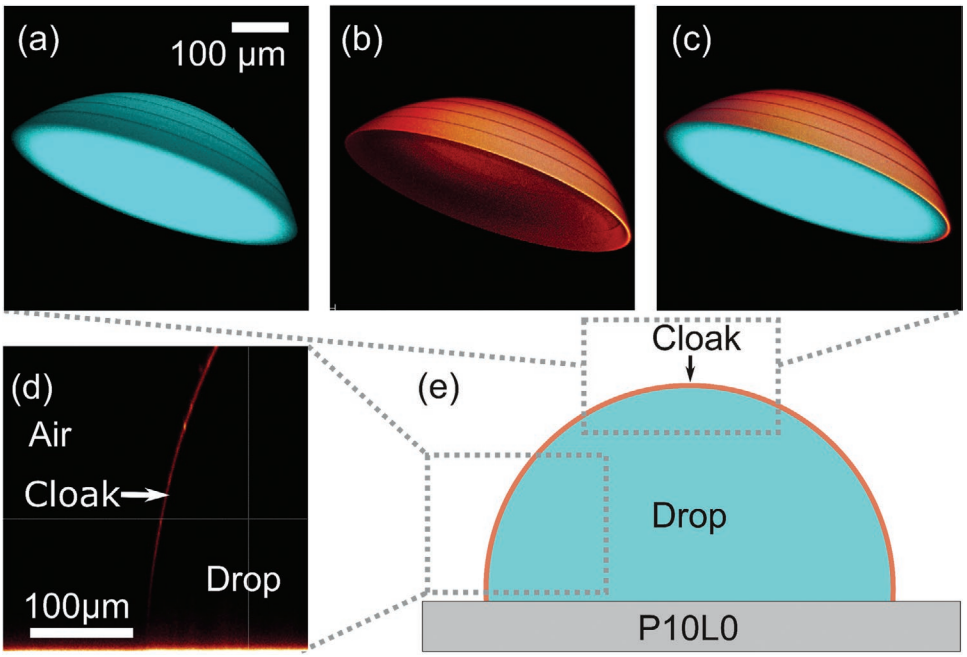

Figure 5. Visualization of the PDMS cloak on a drop using laser scanning confocal microscopy. a–c) show 3D confocal image of the top of a 57% glycerol- 43% water by weight drop (cyan, fluorescent dye: Atto 488; Orange, custom made perylene fluorescent dye) taken ≈30 min after the drop was placed on the surface. (a) shows fluorescent signal from the drop, (b) shows fluorescent signal from the cloak, and (c) is an overlay of (a) and (b). d) 2D cross section of the cloak. e) Schematic of the cloaked drop on P10L0 indicating the location of the images (a–d). The images were taken with a 20 × /0.75 glycerol immersion objective with horizontal resolution of ≈ 0.3 µm and vertical resolution of ≈ 1 µm. Similar result is obtained for visualization of cloaked drop on P10L25.

that of pure water (γ_{wv}). However, due to the positive spreading coefficient of PDMS on water,[48] the drop draws PDMS from the substrate and is cloaked. This results in a decrease in the effective surface tension of the drop-vapor interface from γ_{wv} to $\approx\gamma_{lv} + \gamma_{lw}$. To obtain the interfacial tension of the drop as a function of time [Figure 6b], we imaged the drop's shape and fitted the Young-Laplace equation to its contour [Figure 6c]. As shown in Figure 6b, the surface tension remained unchanged for a certain time, then declined and eventually reached a plateau. This transition can be interpreted as corresponding to the formation of a continuous layer of the lubricant over the droplet surface.[29,50,51] For P10L25, the transition occurred within 30 s whereas for P10L5 it took several minutes. No change in interfacial tension was observed on P10L0 over 30 min. These results clearly show a significant difference in kinetics of cloaking between substrates having different amounts of mobile PDMS molecules arising from the uncrosslinked chains, either due to the bulk lubricant infusion or due to uncrosslinked chains from the Sylgard 184 mixture. Hence, the growing condensate droplets on substrates with bulk lubricant infusion would

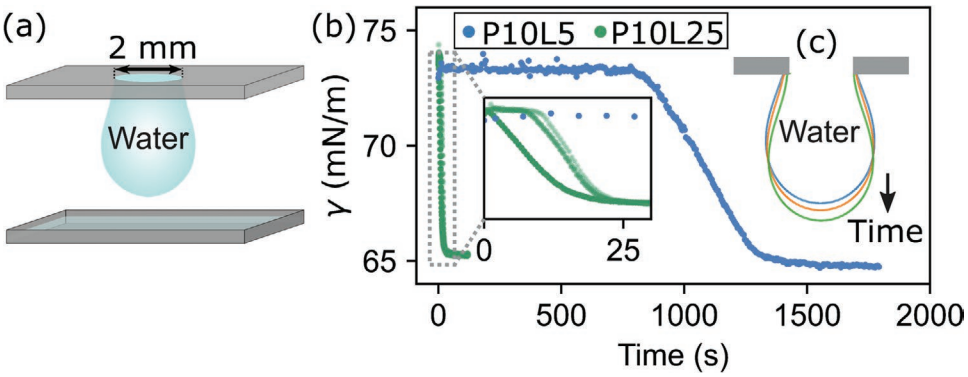

Figure 6. Measuring cloaking timescale using pendant drop method. (a) Schematic of setup. A 2 mm diameter hole was drilled into a glass slide coated with P10L0, P10L5 or P10L25. A water drop (38 µL) was suspended such that the drop's contact line was pinned at the hole's circumference. A water bath was placed a few millimeters below the drop to suppress evaporation. The drop profile was monitored over time, and its surface tension calculated and plotted in (b). The inset in (b) focusses on the transition for P10L25. In the inset, the different green lines correspond to repeats of the same experiment. (c) Evolution of the drop contour over time on P10L25. No change in surface tension was observed on P10L0 over 30 min (see Figure S5, Supporting Information).

© 2021 The Authors. Advanced Functional Materials published by Wiley-VCH GmbH

stay uncloaked for much lesser time thus reducing the overall droplet growth rate compared to substrates without bulk lubricant infusion.

2.5. Dewing

Droplet sliding velocity measurements (Figure 2b and Figure S2 (Supporting Information)) and microscale condensation experiments show that P10L5 and P10L25 show significantly lower viscoelastic dissipation (Table S2, Supporting Information) as well as higher precoalescence growth rate of condensate droplets compared to P1L5, P1L25, and P40L0 (Figure S3b, Supporting Information). Thus we selected P10L5 and P10L25 for water collection performance under dewing. We selected P10L0 as the control substrate for these experiments. We evaluated three different substrates, namely P10L0, P10L5, and P10L25 for water collection through dewing. A custom-designed setup was used to capture the effect of lubrication on water collection rates. P10L25 and P10L5 showed similar average dew water collection rates over the time period of experiment (17 h) and achieve about 44% and 49% higher water collection respectively than P10L0 under similar dewing conditions (**Figure 7**, blue bars). The higher water collection on P10L5 and P10L25 arises from a shorter delay time for the initiation of condensate droplet shedding compared to P10L0 (Figure 7, orange points). Additionally, we calculate that after the onset of droplet shedding, average water collection rate on P10L5 and P10L25 is around 35% higher compared to P10L0. Supporting Information video shows typical dewing on P10L0, P10L5, and P10L25 over the course of one experiment.

The enhanced phase change on PDMS substrates with bulk lubricant infusion show that the higher nucleation density and lower viscoelastic dissipation more than compensate for lower individual droplet growth rate. As a result, it is evident that bulk lubricant infusion is a promising approach to enhance water condensation on soft substrates by reducing viscoelastic braking while retaining the inherent high nucleation density.

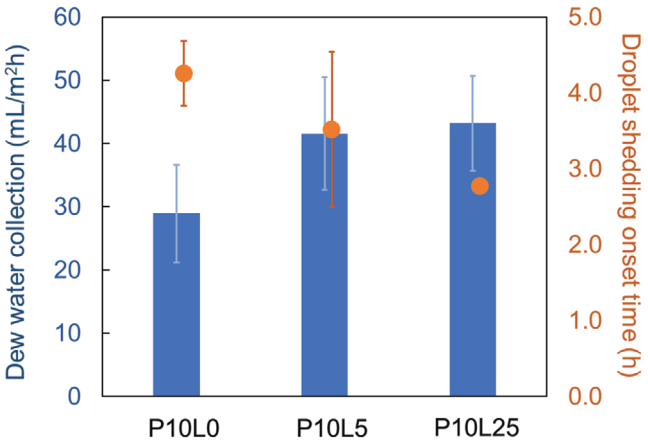

Figure 7. Dew water collection rate (blue bars) and onset time for droplet shedding (orange points) on P10L0, P10L5, and P10L25. Each bar and dot represents an average over four experiments with each experiment conducted over a period of 17 h. Error bars represent standard deviation over these experiments. Condensation occurs on the samples under an atmospheric relative humidity of 68.6%, air temperature of 16.6 °C and copper plate surface temperature of 2.1 °C (mean values across four experiments). Dew water collection rate is average rate over the period of experiment. Droplet shedding time represents the time from start of experiment when the first condensate drop sheds from the substrate.

We have further compared the dewing performance on PDMS substrates against a rigid hydrophobic planar copper substrate. We chose P10L0 for this comparison as it is the highest shear modulus among the PDMS substrates considered in this work.[43] Although the nucleation densities shown in Figure 3 are low compared to the typical values reported on metallic substrates,[52,53] we emphasize here that, in addition to the rigidity of the substrate, the nucleation density during condensation is also sensitive to other factors such as surface roughness, level of subcooling[54] and fraction of non-condensable gases in water vapor.[55] Additionally the thermal conductivity of these soft organogels of around 0.2 W mK^{-1}[56,57] is much lower compared to metals, such as Copper and Aluminium, that are typically used in heat transfer applications. Thus we have compared the dewing performance of P10L0 and hydrophobic copper substrates under same atmospheric humidity and subcooling conditions.[43] The rigid hydrophobic Cu substrate shows 54% lower dew collection than P10L0 at same level of subcooling. The higher dewing performance on P10L0 arises from the inherently high nucleation density and lower contact angle hysteresis compared to the hydrophobic rigid Copper substrate.[17,43] (Refer Section S9 in the Supporting Information for further details of this experiment). Thus, at similar level of subcooling, a rigid hydrophobic substrate with contact angle hysteresis lower than P10L0 would be required to achieve higher dewing performance.[43]

Due to the higher thermal resistance of these organogels compared to metals, these soft substrates are not suitable for active cooling applications when used as bulk materials. However we envisage that these materials can be utilized in the form of thin composite coatings embedded with high thermal conductivity materials, such as liquid metal nanodroplets,[58] to improve the overall condensation heat transfer in metallic condensers.[43] Additionally, PDMS substrates of thickness above 100 µm can passively radiate heat to space and thus can be utilized for dew water harvesting during night as well as day.[59–61] Hence, these PDMS based organogels can potentially replace traditional PDMS based emitters in such applications to improve the overall dew harvesting potential.

We recognize that the collected water as a result of dewing on these organogels would contain a finite fraction of uncrosslinked chains from PDMS and lubricant due to shedding of cloaked water droplets. However, such lubricant loss is likely to be a small fraction of the overall weight of the substrate.[36] In order to verify this aspect, we have performed an extended dewing experiment wherein P10L25 was exposed to dewing for ≈111 h. We found that only about 0.11% by weight of the lubricant contained within the sample was depleted from the sample during this time. This translates to an average rate of lubricant addition in water of 0.011% per hour by volume of water condensed on the substrate. (refer Section S9 in the Supporting Information for details of the extended dewing experiment). This small amount of lubricant may be removable to ensure water potability, if so desired, by adopting one of the existing approaches for energy efficient oil/water separation.

© 2021 The Authors. Advanced Functional Materials published by Wiley-VCH GmbH

These include use of metallic meshes or fabrics with tuned wettability and chemically functionalized 3D porous materials such as nanocomposite aerogels.[62,63]

3. Conclusion

We demonstrate that water condensation on soft substrates can be significantly enhanced through bulk lubricant infusion in PDMS. Lubricant infusion in PDMS reduces the shear modulus and increases the fraction of uncrosslinked chains in the substrate. GPC analysis shows that the mobile chains in such substrates are dominated by the low molecular weight components of the crosslinker and base and by the additional lubricant. Additionally, a mere 5% by weight lubricant infusion reduces the viscoelastic dissipation in the substrate by nearly 28 times compared to crosslinked PDMS with stoichiometric composition. Moreover, lubricant infusion in stoichiometric PDMS composition provides the most benefit in terms of achieving slippery soft substrates compared to lubricant infusion in non-stoichiometric PDMS composition. Lubricant infused PDMS also achieves a higher density of droplet nucleation during condensation. However, individual condensate droplet growth rate through direct condensation is reduced on such substrates due to cloaking of the condensate droplets with the lubricant. The nucleation density and droplet growth rate are observed to be rather insensitive to the amount of lubricant in the substrate. Overall, slippery soft substrates, obtained by bulk lubricant infusion in PDMS, achieved up to 49% higher rate of water condensation compared to PDMS without any additional lubricant. The overall effect of bulk lubricant infusion in terms of enhancing the rate of water condensation provides an important pathway for realistic application of soft substrates in water condensation applications.

4. Experimental Section

Materials and Sample Preparation: PDMS (Sylgard 184, Dow Corning and lubricant (silicone oil, Xiameter PMX 200, 100 cSt, Credimex Inc.) were used to prepare the test substrates. For each sample, the base, the crosslinking agent and the lubricant were first thoroughly mixed in the desired weight ratio and then degassed for 15 to 20 min in a vacuum desiccator to remove air bubbles. Subsequently, the mixture was poured into a mold and then cured in an oven at 80 °C for 2 h. The thickness of all samples was 2 mm. In essence, our samples can be regarded as bulk PDMS. In order to ensure consistent curing conditions for all samples, we scheduled our experiments such that sample storage time between the end of curing and the start of experiments was maintained nearly the same across all the samples.

Measurement of Uncrosslinked Chains Fraction and Molecular Weight Distribution: The relative amount and the molecular weight distribution of the uncrosslinked chains was determined by dissolving out the oligomers in toluene. Each sample was kept immersed in a beaker with ≈450–600 ml toluene, which was stirred at 200 rpm (round per minute) for ten days. During this period, uncrosslinked chains diffused into toluene, which is a good solvent for PDMS, the curing agent and silicone oil. The toluene was renewed at the end of the 5th and the 7th day of immersion. Subsequently, the sample was immersed in hexane for seven days, wherein the hexane was renewed at the end of the 2nd and 4th day. Hexane is more volatile than toluene which helps in the eventual drying of the sample. The sample was dried under a fume hood for one night, in the oven at 50 °C, and eventually under vacuum for about 7 to 8 h. Finally, the sample was cooled at room temperature and weighed again to calculate the fraction of uncrosslinked chains. Additionally, we performed GPC analysis in order to determine the composition of uncrosslinked chains in various PDMS substrates. For each sample, Gel Permeation Chromatography (GPC) analysis was performed using the toluene from first extraction which yielded the molecular weight distribution of the uncrosslinked chains extracted from that sample. (refer to Section S1 in the Supporting Information for details on GPC analysis).

Characterization of Substrate Elasticity: The elasticity of each sample was characterized by using a micro-indentation test. This test enabled the measurement of the Young's modulus (E) of the substrate and was performed using the micromechanical testing station FT-MTA02 (FemtoTools AG, Buchs ZH, Switzerland). The substrate shear modulus G is related to elastic modulus as $G = E/2(1 + \nu)$, where ν is the Poisson's ratio of the material. For elastomers, this relationship can be simplified to $E = 3G$.[24] (refer to Section S5 in the Supporting Information for further details).

Measurement of Wetting Ridge Height: The wetting ridge height was measured by using a white light interferometer (Zygo Inc.).[39] For these measurements, droplets of ethylene glycol (Sigma Aldrich) dyed with 2.6% by weight Sudan IV (Sigma Aldrich) were used.[64] The higher boiling point of ethylene glycol compared to water minimizes droplet evaporation at room temperature during the wetting ridge height measurements which minimizes any change in droplet size due to evaporation during the measurement. Ethylene glycol has a similar order of magnitude surface tension as water (47 mN m^{-1}). Since the measured wetting ridge height is a function of droplet size,[65] measurements for each substrate were repeated with droplets of multiple sizes ranging from ≈4 to ≈20 µL to ensure consistent comparison between substrates (see Figure S7 in the Supporting Information).

Viscoelastic Dissipation in the Substrate: We characterized the viscoelastic dissipation of each substrate by letting small droplets of a range of sizes to slide on a soft substrate.[25,64] In our experiments, 0.5 to 3.5 µL droplets of ethylene glycol were allowed to slide on vertically oriented substrates while their motion was carefully monitored using a CMOS camera. The higher boiling point of ethylene glycol minimized any change in droplet size due to evaporation as the droplet slid on the substrate. For each droplet size, the droplet was deposited on the vertically oriented substrate. The droplet started sliding downwards and the droplet velocity was measured when it attained a constant (terminal) sliding velocity. For repeatability, two samples of each type were fabricated and tested under the same conditions. Further details are provided in Section S7 in the Supporting Information.

Microscale Condensation: The sample was enclosed in a custom-designed chamber for observations under an optical microscope (refer to Figure S9 in the Supporting Information for a schematic of the experimental setup). Inside the chamber, an environment with 100% relative humidity was maintained by placing water-saturated paper wipes. The sample temperature was controlled by mounting it on a temperature-controlled microscope stage (BCS-196, Linkam Scientific) using a copper stub and thermal paste. In order to avoid influencing the condensation process and due to the softness of PDMS organogel samples, temperature sensor was not mounted directly on the top surface of the substrate. The similar thermal conductivity of silicone oil (≈0.15 W mK^{-1}[66]) and PDMS (≈0.16 – 0.18 W mK^{-1}[56,57]) ensured consistent subcooling across the various substrates. The humidity and temperature of the environment inside the chamber were continuously monitored using a humidity sensor (HYT221, IST Inc.) and a temperature sensor (PT10000, IST Inc.). The condensation process was recorded with a CMOS camera, and the recorded videos were analyzed to determine nucleation density and droplet growth rate. Once the sample was in position, the chamber was sealed, and the temperature-controlled stage was set to 35 °C in order to induce evaporation of water from wet paper wipes. Once a stable humidity level of 100% was achieved, the temperature setpoint of the stage was reduced to 20 °C to initiate condensation. Image acquisition was initiated as soon as the smallest droplet resolvable by the microscope appeared on the substrate. The imaging was continued at a constant acquisition

© 2021 The Authors. Advanced Functional Materials published by Wiley-VCH GmbH

rate until droplets started coalescing. It was ensured that all samples were tested under a consistent humid air chamber atmospheric temperature of 28.7 ± 0.5 °C. For each sample, at least three independent measurements of nucleation density and droplet growth rate were obtained.

Cloaking: We used a laser scanning confocal fluorescent microscope (Leica TCS SP8) to directly visualize the cloaking layer covering drops and confirm this effect for PDMS samples with and without additional bulk lubricant infusion. Fluorescent dye (excitation maximum $\lambda_{ex} = 663$ nm, emission maximum $\lambda_{em} = 712$ nm) was added to the PDMS mixture during sample preparation. The mixture was spin-coated for 1 min at 1100 rounds per minute onto 170 µm thick microscope coverslips. PDMS films were allowed to crosslink at 80 °C for two hours. Afterwards, a 0.3 µL drop of 57% water and 43% glycerol (fluorescently labelled with Atto 488: $\lambda_{ex} = 504$ nm and $\lambda_{em} = 521$ nm) was placed and left for 30 min to ensure enough time for the formation of any cloaking layer. The addition of glycerol reduced evaporation and improved refractive index matching with PDMS, thus reducing undesired optical artefacts ($n_{water} = 1.33$, $n_{glycerol} = 1.47$, $n_{drop} = 1.41$, $n_{PDMS} = 1.41$, n: refractive index). Subsequently, the top part of the drop was visualized with a 20 ×/0.75 glycerol immersion objective using an argon 488 nm laser to excite the dye in the drop and a helium-neon 633 nm laser to excite the dye in the PDMS. The emitted fluorescent signals were simultaneously captured by separate detectors, and a final image showing the signal from each fluorescent dye was constructed.

Dewing: Substrates were tested for water collection through dewing by using a custom-designed setup. In a dewing experiment, PDMS substrates with and without bulk lubricant infusion were tested together so as to achieve consistent temperature and humidity conditions across the samples. The tested substrates were fabricated by crosslinking directly on a copper plate to ensure good thermal contact between PDMS samples and copper. Each sample was fabricated to be 2 mm thick. The copper plate with the samples was then mounted onto a vertically oriented Peltier cooler and subsequently the samples were exposed to humid air in a closed chamber. The humidity inside the chamber was maintained at ≈68.6% by injecting humid air generated by passing compressed air through a bubbler. The Peltier cooler was set such that the copper plate surface temperature was maintained at ≈2.1 °C. The resulting condensation on the samples was monitored by using a DSLR camera, and water condensed on the substrates was collected. Each experiment was run for ≈17 h, and copper plate surface temperature, chamber temperature, and humidity were continuously monitored. Subsequently, the collected water from each sample was weighed. An extended dewing experiment was also performed on P10L25 substrate to determine any lubricant depletion due to condensation on the substrate. In this experiment, the substrate was exposed to dewing for ≈111 h. (Refer Section S9 in the Supporting Information for further details on dewing experiments).

Supporting Information

Supporting Information is available from the Wiley Online Library or from the author.

Acknowledgements

The authors thank Peter Feusi and Jovo Vidic for their help with the experimental setup assembly as well as Dr. Hadi Eghlidi for inputs on optical observations. This project has received funding from the European Union's Horizon 2020 research and innovation program under grant number 801229 (HARMoNIC), the innovative training network LubISS under the grant number 722497 (A.N., M.D'.A., D.V.), and the Commission for Technology and Innovation, (CTI) under the Swiss Competence Centers for Energy Research (SCCER) program (Grant No. KTI.2014.0148).

Open access funding provided by Eidgenossische Technische Hochschule Zurich.

Conflict of Interest

The authors declare no conflict of interest.

Data Availability Statement

The data that support the findings of this study are available in the supplementary material of this article.

Keywords

cloaking, condensation, lubricant infused, PDMS, soft substrate

Received: September 23, 2021
Revised: November 23, 2021
Published online: December 29, 2021

[1] J. M. Beér, *Prog. Energy Combust. Sci.* **2007**, *33*, 107.
[2] D. González, J. Amigo, F. Suárez, *Renew. Sustainable Energy Rev.* **2017**, *80*, 238.
[3] P.-B. Bintein, H. Lhuissier, A. Mongruel, L. Royon, D. Beysens, *Phys. Rev. Lett.* **2019**, *122*, 98005.
[4] C. S. Sharma, C. W. E. Lam, A. Milionis, H. Eghlidi, D. Poulikakos, *ACS Appl. Mater. Interfaces* **2019**, *11*, 27435.
[5] M. Edalatpour, K. R. Murphy, R. Mukherjee, J. B. Boreyko, *Adv. Funct. Mater.* **2020**, *30*, 2004451.
[6] J. W. Rose, *Proc. Inst. Mech. Eng. Part A J. Power Energy* **2002**, *216*, 115.
[7] R. Enright, N. Miljkovic, J. L. Alvarado, K. Kim, J. W. Rose, *Nanoscale Microscale Thermophys. Eng.* **2014**, *18*, 223.
[8] C. S. Sharma, J. Combe, M. Giger, T. Emmerich, D. Poulikakos, *ACS Nano* **2017**, *11*, 1673.
[9] J. B. Boreyko, C.-H. Chen, *Phys. Rev. Lett.* **2009**, *103*, 184501.
[10] M. Donati, C. W. E. Lam, A. Milionis, C. S. Sharma, A. Tripathy, A. Zendeli, D. Poulikakos, *Adv. Mater. Interfaces* **2021**, *8*, 2001176.
[11] H. Vahabi, W. Wang, J. M. Mabry, A. K. Kota, *Sci. Adv.* **2018**, *4*, eaau3488.
[12] N. Miljkovic, R. Enright, Y. Nam, K. Lopez, N. Dou, J. Sack, E. N. Wang, *Nano Lett.* **2012**, *13*, 179.
[13] X. Chen, R. S. Patel, J. A. Weibel, S. V Garimella, *Sci. Rep.* **2016**, *6*, 18649.
[14] X. Chen, J. Wu, R. Ma, M. Hua, N. Koratkar, S. Yao, Z. Wang, *Adv. Funct. Mater.* **2011**, *21*, 4617.
[15] A. Aili, H. Li, M. H. Alhosani, T. Zhang, *ACS Appl. Mater. Interfaces* **2016**.
[16] J. Zhu, Y. Luo, J. Tian, J. Li, X. Gao, *ACS Appl. Mater. Interfaces* **2015**, *7*, 10660.
[17] C. S. Sharma, C. Stamatopoulos, R. Suter, P. R. Von Rohr, D. Poulikakos, *ACS Appl. Mater. Interfaces* **2018**, *10*, 29127.
[18] C. Lv, P. Hao, X. Zhang, F. He, *ACS Nano* **2015**, *9*, 12311.
[19] D. Seo, J. Lee, C. Lee, Y. Nam, *Sci. Rep.* **2016**, *6*, 24276.
[20] A. Lee, M.-W. Moon, H. Lim, W.-D. Kim, H.-Y. Kim, *Langmuir* **2012**, *28*, 10183.
[21] M. Sokuler, G. K. Auernhammer, M. Roth, C. Liu, E. Bonacurrso, H.-J. Butt, *Langmuir* **2010**, *26*, 1544.
[22] F. Eslami, J. A. W. Elliott, *J. Phys. Chem. B* **2011**, *115*, 10646.
[23] E. R. Jerison, Y. Xu, L. A. Wilen, E. R. Dufresne, *Phys. Rev. Lett.* **2011**, *106*, 186103.
[24] M. E. R. Shanahan, A. Carré, *Colloids Surf., A* **2002**, *206*, 115.
[25] S. Karpitschka, S. Das, M. van Gorcum, H. Perrin, B. Andreotti, J. H. Snoeijer, *Nat. Commun.* **2015**, *6*, 7891.

© 2021 The Authors. Advanced Functional Materials published by Wiley-VCH GmbH

[26] T.-S. Wong, S. H. Kang, S. K. Y. Tang, E. J. Smythe, B. D. Hatton, A. Grinthal, J. Aizenberg, *Nature* **2011**, *477*, 443.
[27] A. Lafuma, D. Quéré, *EPL* **2011**, *96*, 56001.
[28] S. Anand, A. T. Paxson, R. Dhiman, J. D. Smith, K. K. Varanasi, *ACS Nano* **2012**, *6*, 10122.
[29] S. Anand, K. Rykaczewski, S. B. Subramanyam, D. Beysens, K. K. Varanasi, *Soft Matter* **2015**, *11*, 69.
[30] X. Dai, N. Sun, S. O. Nielsen, B. B. Stogin, J. Wang, S. Yang, T.-S. Wong, *Sci. Adv.* **2018**, *4*, eaaq0919.
[31] P. Kim, M. J. Kreder, J. Alvarenga, J. Aizenberg, *Nano Lett.* **2013**, *13*, 1793.
[32] P. Zhang, C. Zhao, T. Zhao, M. Liu, L. Jiang, *Adv. Sci.* **2019**, *6*, 1900996.
[33] K. Golovin, S. P. R. Kobaku, D. H. Lee, E. T. DiLoreto, J. M. Mabry, A. Tuteja, *Sci. Adv.* **2016**, *2*, 1501496.
[34] L. Zhu, J. Xue, Y. Wang, Q. Chen, J. Ding, Q. Wang, *ACS Appl. Mater. Interfaces* **2013**, *5*, 4053.
[35] Y. H. Yeong, A. Milionis, E. Loth, J. Sokhey, *Cold Reg. Sci. Technol.* **2018**, *148*, 29.
[36] A. Hourlier-Fargette, A. Antkowiak, A. Chateauminois, S. Neukirch, *Soft Matter* **2017**, *13*, 3484.
[37] P.-G. de Gennes, F. Brochard-Wyart, D. Quéré, *Capillarity and Wetting Phenomena*, Springer, Cham, Switzerland **2004**.
[38] R. W. Style, E. R. Dufresne, *Soft Matter* **2012**, *8*, 7177.
[39] A. Carre, J.-C. Gastel, M. E. R. Shanahan, *Nature* **1996**, *379*, 432.
[40] J. T. Pham, F. Schellenberger, M. Kappl, H.-J. Butt, *Phys. Rev. Mater.* **2017**, *1*, 15602.
[41] W. S. Y. Wong, L. Hauer, A. Naga, A. Kaltbeitzel, P. Baumli, R. Berger, M. D'Acunzi, D. Vollmer, H.-J. Butt, *Langmuir* **2020**, *36*, 7236.
[42] A. Keiser, P. Baumli, D. Vollmer, D. Quéré, *Phys. Rev. Fluids* **2020**, *5*, 14005.
[43] A. Phadnis, K. Rykaczewski, *Langmuir* **2017**, *33*, 12095.
[44] M. Sokuler, G. K. Auernhammer, C. J. Liu, E. Bonaccurso, H.-J. Butt, *EPL* **2010**, *89*, 36004.
[45] H. Masoud, P. D. Howell, H. A. Stone, *J. Fluid Mech.* **2021**, *927*, R4.
[46] F. Schellenberger, J. Xie, N. Encinas, A. Hardy, M. Klapper, P. Papadopoulos, H.-J. Butt, D. Vollmer, *Soft Matter* **2015**, *11*, 7617.
[47] I. O. Ucar, H. Y. Erbil, *Colloids Surf., A* **2012**, *411*, 60.
[48] J. D. Smith, R. Dhiman, S. Anand, E. Reza-Garduno, R. E. Cohen, G. H. McKinley, K. K. Varanasi, *Soft Matter* **2013**, *9*, 1772.
[49] A. Naga, A. Kaltbeitzel, W. S. Y. Wong, L. Hauer, H.-J. Butt, D. Vollmer, *Soft Matter* **2021**, *17*, 1746.
[50] I. Langmuir, *J. Am. Chem. Soc.* **1917**, *39*, 1848.
[51] V. Bergeron, D. Langevin, *Phys. Rev. Lett.* **1996**, *76*, 3152.
[52] C. Graham, P. Griffith, *Int. J. Heat Mass Transfer* **1973**, *16*, 337.
[53] J. W. Rose, *Int. J. Heat Mass Transfer* **1976**, *19*, 1363.
[54] C. Mu, J. Pang, Q. Lu, T. Liu, *Chem. Eng. Sci.* **2008**, *63*, 874.
[55] D. Niu, H. Gao, G. Tang, Y. Yan, *Langmuir* **2021**, *37*, 9009.
[56] J. Wei, M. Liao, A. Ma, Y. Chen, Z. Duan, X. Hou, M. Li, N. Jiang, J. Yu, *Compos. Commun.* **2020**, *17*, 141.
[57] P. Yi, R. A. Awang, W. S. T. Rowe, K. Kalantar-zadeh, K. Khoshmanesh, *Lab Chip* **2014**, *14*, 3419.
[58] M. D. Bartlett, N. Kazem, M. J. Powell-Palm, X. Huang, W. Sun, J. A. Malen, C. Majidi, *Proc. Natl. Acad. Sci.* **2017**, *114*, 2143 LP.
[59] L. Zhou, H. Song, J. Liang, M. Singer, M. Zhou, E. Stegenburgs, N. Zhang, C. Xu, T. Ng, Z. Yu, B. Ooi, Q. Gan, *Nat. Sustainability* **2019**, *2*, 718.
[60] M. Zhou, H. Song, X. Xu, A. Shahsafi, Y. Qu, Z. Xia, Z. Ma, M. A. Kats, J. Zhu, B. S. Ooi, Q. Gan, Z. Yu, *Proc. Natl. Acad. Sci.* **2021**, *118*, 2019292118.
[61] H. Iwan, P. Hyunchul, S. Gabriel, G. Tobias, R. Mathieu, T. Abinash, M. Athanasios, S. T. M, P. Dimos, *Sci. Adv.* **2021**, *7*, eabf3978.
[62] R. K. Gupta, G. J. Dunderdale, M. W. England, A. Hozumi, *J. Mater. Chem. A* **2017**, *5*, 16025.
[63] H. Liu, X. Chen, Y. Zheng, D. Zhang, Y. Zhao, C. Wang, C. Pan, C. Liu, C. Shen, *Adv. Funct. Mater.* **2021**, *31*, 2008006.
[64] S. Karpitschka, A. Pandey, L. A. Lubbers, J. H. Weijs, L. Botto, S. Das, B. Andreotti, J. H. Snoeijer, *Proc. Natl. Acad. Sci.* **2016**, *113*, 7403.
[65] R. W. Style, R. Boltyanskiy, Y. Che, J. S. Wettlaufer, L. A. Wilen, E. R. Dufresne, *Phys. Rev. Lett.* **2013**, *110*, 66103.
[66] XIAMETER™ PMX-200 Silicone Fluid 100 cSt.

© 2021 The Authors. Advanced Functional Materials published by Wiley-VCH GmbH